Solution Structure and Folding Characteristics of the C-Terminal SH3 Domain of c-Crk-II[†,‡]

Vasant Muralidharan,[§,||] Kaushik Dutta,[||,⊥] Jaehyun Cho,[#] Miquel Vila-Perello,[§] Daniel P. Raleigh,[#,¶] David Cowburn,[⊥] and Tom W. Muir*[,§]

Laboratory of Synthetic Protein Chemistry, The Rockefeller University, New York, New York 10021, New York Structural Biology Center, 89 Convent Avenue, New York, New York 10027, and Graduate Program in Biochemistry and Structural Biology and Department of Chemistry, State University of New York—Stony Brook, Stony Brook, New York 11794

Received March 24, 2006; Revised Manuscript Received May 15, 2006

ABSTRACT: Crk-II is a signaling adaptor protein that is involved in many cellular processes including apoptosis, proliferation, and differentiation. It has a modular domain architecture consisting of an Src homology 2 domain (SH2) followed by two Src homology 3 (SH3) domains. The structures and ligand-binding properties of the SH2 and the middle SH3 domains are well-characterized. Several studies suggest that the C-terminal SH3 domain plays an important regulatory role in the protein; however, no structural information is available on this domain, and relatively little is known about its binding partners. In the current work, we have solved the solution NMR structure of the C-terminal SH3 domain. The domain adopts the standard SH3 fold comprising a five-stranded β barrel. In agreement with alignment and modeling studies, the structure indicates that the canonical-binding surface of the SH3 domain is unusually polar and suggests that this domain may not bind typical PXXP ligands or that it may bind them with reduced affinity. Thermodynamic and kinetic studies show that the domain folds in a reversible two-state manner and that the stability of the fold is similar to that observed for other SH3 domains. These studies offer some insight into the likely structural and thermodynamic consequences of point mutations in the cSH3 domain that are known to deregulate Crk-II function. Our results set the stage for a better understanding the role of the cSH3 domain in the context of the full-length protein.

The Crk family of signaling adaptor proteins has been implicated in many cellular processes such as proliferation, adhesion, and motility (*1*−*8*). Alternative splicing of the *c-crk* gene yields two different translation products, Crk-II (∼300 residues) and Crk-I (∼200 residues). The Crk-II isoform is the more widely expressed and contains a Src homology 2 (SH2) domain followed by two Src homology 3 (SH3) domains, whereas Crk-I lacks the C-terminal SH3 domain (*9*, *10*). The related protein Crk-L has a similar architecture to Crk-II (*11*).

The primary role of Crk-II as a scaffolding protein is to bring together signaling proteins that bind to the SH2 and SH3 modular interaction domains. Accordingly, the SH2 domain recognizes pY-X-X-P motifs and mediates interactions with several proteins such as p130[cas], Cbl kinase, and paxillin (*5*, *12*−*14*). In addition, the linker region between the two SH3 domains of Crk-II contains the motif Y^{221}-A-Q-P, which can be phosphorylated by the protein tyrosine kinase, c-Abl, creating an intramolecular docking site for the Crk-SH2 domain (*15*). This triggers a structural change in the protein that is thought to regulate its function (*16*). The Crk-II SH2 domain is unique in that it contains a proline-rich insertion within a surface loop that serves as a ligand for the SH3 domain of c-Abl (*17*, *18*). The solution structure of the Crk-II SH2 domain in complex with the Abl-SH3 domain and the Crk-derived phosphotyrosine peptide has been determined and provides insights into the regulation of the two binding interactions involving the SH2 domain (*18*). The central SH3 domain of Crk-II (hereafter referred to as nSH3) has also been well-characterized at the structural (*19*) and biochemical (*20*, *21*) levels. The domain recognizes P-X-X-P-X-K sequences and has been shown to interact with several proteins including the guanine nucleotide exchange factor, C3G (*22*), DOCK180 (*23*), and c-Abl (*24*).

In comparison to the SH2 and nSH3 domains, the structure and function of the putative C-terminal SH3 domain of c-Crk-II is poorly understood (hereafter referred to as cSH3).[1] The sequence of this region of the protein is highly conserved in organisms ranging from fruit fly to man, suggesting that

[†] This work was supported in part by the National Health Institute Grants (GM-55843-07, to T.W.M., GM-70941 to D.P.R., and GM-47021 and GM-66356, to D.C.).

[‡] The coordinates have been deposited in the Protein Data Bank (PDB) with PDB accession code 2GGR and as BioMagResBank entry 7129.

* To whom correspondence should be addressed: Box 223, The Rockefeller University, 1230 York Avenue, NY 10021. Telephone: 212-327-7368. Fax: 212-327-7358. E-mail: muirt@rockefeller.edu.

[§] Laboratory of Synthetic Protein Chemistry, The Rockefeller University.

[||] These authors contributed equally to this work.

[⊥] New York Structural Biology Center.

[#] Graduate Program in Biochemistry and Structural Biology, State University of New York—Stony Brook.

[¶] Department of Chemistry, State University of New York—Stony Brook.

[1] Abbreviations: cSH3, C-terminal SH3 domain of Crk-II; NES, nuclear export sequence.

10.1021/bi060590z CCC: $33.50
Published on Web 06/29/2006

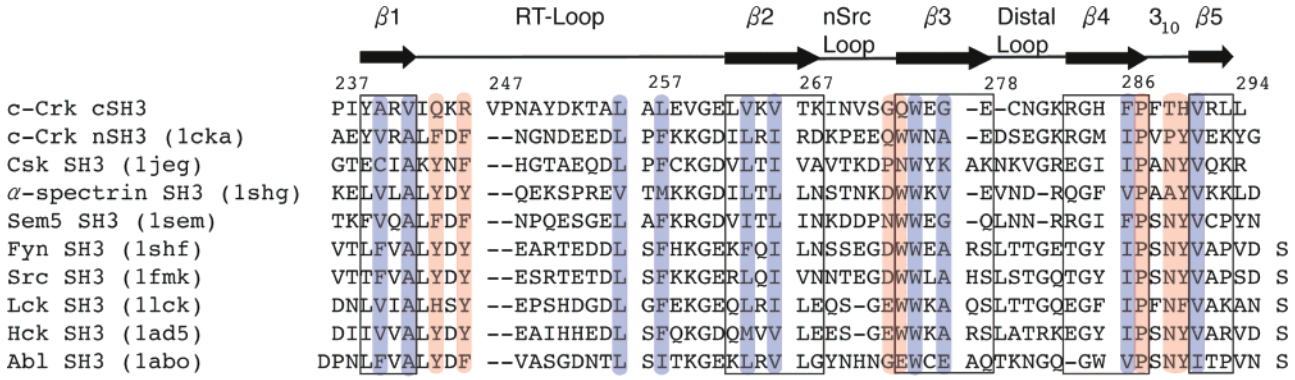

FIGURE 1: Sequence and secondary-structure alignment of SH3 domains including the cSH3 domain. Conserved residues involved in ligand binding are highlighted in orange boxes, and conserved residues of the hydrophobic core are highlighted in blue boxes. The PDB codes are in parentheses.

the domain plays an important functional role. Indeed, point mutations or deletions in the cSH3 domain are known to perturb a number of cellular processes, including proliferation (*7*, *25*), adhesion (*4*, *26*), and endocytosis (*27*, *28*). Moreover, overexpression of Crk-I, which resembles the viral oncogene v-Crk (*29*), transforms fibroblasts in culture (*10*). These studies have led to the hypothesis that the cSH3 domain negatively regulates the function of Crk-II (*5*). Further advancement of this model has been frustrated by the inability to find classical P-X-X-P-containing protein ligands for the cSH3 domain (*5*). Although sequence alignment analyses strongly predict that the cSH3 is a canonical SH3 domain (*30*), many of the conserved aromatic residues that constitute the ligand-binding surface in the SH3 domain family are replaced by polar, typically nonaromatic residues in the cSH3 domain (Figure 1). This raises the possibility that the cSH3 domain does not bind typical P-X-X-P ligands or that it binds them with reduced affinity.

The only documented interaction partner for the cSH3 domain is the nuclear exportin, Crm-1, which is believed to bind to a putative nuclear export sequence (NES, residues L256−V266) within the domain (*31*). Interestingly, on the basis of sequence alignment analysis (*30*), the predicted NES forms part of the central β barrel in the protein and, furthermore, four of the residues (L256, L258, V264, and V266) are expected to be in the hydrophobic core of the protein (Figure 1). Thus, the mechanism by which Crm-1 recognizes this NES in the context of the native cSH3 structure is unclear.

As a first step toward understanding the role of the cSH3 domain in regulating Crk-II function, we have carried out a series of structural and biophysical studies on the isolated domain. The solution nuclear magnetic resonance (NMR) structure of the cSH3 domain has been determined and reveals a standard SH3 β-barrel fold in which a three-stranded antiparallel β sheet packs orthogonally against a two-stranded antiparallel β sheet. The structure indicates that the canonical P-X-X-P-binding surface of the cSH3 domain is indeed unusually polar and that the putative Crm-1-binding motif is buried within the core of the protein. Thermodynamic and kinetic studies show that the cSH3 domain folds in a reversible two-state manner and that the stability of the fold is similar to that observed for other SH3 domains. These studies offer insight into the likely structural and thermodynamic consequences of point mutations in the cSH3 domain that are known to deregulate Crk-II function. Overall, our results also set the stage for a fuller understanding of the role of the cSH3 domain in the context of the full-length protein.

EXPERIMENTAL PROCEDURES

General Methods. All chemicals were purchased from Sigma−Aldrich Chemical Co. (St. Louis, MO). Restriction endonucleases were purchased from New England Biolabs (Beverly, MA). Analytical reverse-phase high-performance liquid chromatography (RP-HPLC) was carried out using a Hewlett−Packard 1100 series instrument with 214 and 280 nm detection. The column used for analytical RP-HPLC was a Vydac C18 column with a constant flow rate of 1 mL/min. All runs used a linear gradient of buffer A [0.1% (v/v) aqueous TFA] versus buffer B [0.1% TFA (v/v) and 90% (v/v) acetonitrile]. Electrospray mass spectrometry (ESMS) was performed on a Sciex API-100 single-quadrupole electrospray mass spectrometer.

Cloning and Protein Expression. The cSH3 domain (residues L230−S304) was isolated from Crk-II cDNA by a polymerase chain reaction (PCR) using a 5′ primer (5′-CCGCTCGAGGAGAACCTGTACTTCCAGGGCCTC-CCTAACCTCCAGAATGGGCCCATTTATGCCAGG-3′) encoding a *Xho*I restriction site and a 3′ primer (5′-CCCAAGCTTTCAGCTGAAGTCCTCATCGGG-3′) encoding a *Hin*dIII restriction site. The 5′ primer also encoded a polyhistidine tag and a Tev protease site. The PCR product was introduced into a pTrcHis plasmid (Invitrogen) using *Xho*I and *Hin*dIII restriction sites. The resulting plasmid, pTrcHis-Tev-cSH3, was free of mutations in the protein-encoding region based on DNA sequencing. The plasmid, pTrcHis-Tev-cSH3, encodes a Tev protease cleavage site between the polyhistidine tag and the cSH3 domain. For expression of the unlabeled cSH3 domain, the plasmid was transformed into *Escherichia coli* BL21 cells (Invitrogen) and were grown to mid-log phase in Luria−Bertani medium containing 100 μg/mL ampicillin. The protein expression was induced with the addition of 1 mM isopropyl-β-D-thiogalactopyranoside (IPTG) at 37 °C for 6 h. The cells were then lysed by passage through a French press. The uniformly ^{13}C- and ^{15}N-labeled cSH3 domain was produced using the same procedure as above, except the cells were grown in M9 minimal media supplemented with 2 g/L ^{13}C glucose and 1 g/L $^{15}NH_4Cl$ (Isotec) as the sole carbon and nitrogen sources, respectively. The His-tagged protein was then purified by

affinity chromatography using Ni^{2+}-NTA resin (Novagen) and dialyzed into Tev cleavage buffer [20 mM Tris at pH 8, 0.5 mM ethylenediaminetetraacetic acid (EDTA), and 1 mM dithiothreitol (DTT)]. Cleavage of the polyhistidine tag by Tev protease (Invitrogen) results in the addition of a glycine residue at the N terminus of the cSH3 domain. Tev cleavage was initiated by the addition of 1 unit of protease per 50 μg of fusion protein. After 3 days, the cleaved product, cSH3, was purified by ion-exchange chromatography using a HiTrap Q sepharose column (Amersham Biosciences) and a linear gradient of 10 mM Tris at pH 7.5 versus 10 mM Tris at pH 7.5 and 1 M NaCl at a flow rate of 1 mL/min. The purity of the cSH3 domain was assessed to be >95% by HPLC and ESMS (Figure S1 in the Supporting Information). The purified cSH3 domain was dialyzed into the NMR buffer [10 mM sodium phosphate at pH 7.2, 50 mM NaCl, 5 mM DTT-d_{10}, 0.1% NaN_3, 1 mM EDTA, and protease inhibitor cocktail (Roche)] and concentrated to 0.3−0.4 mM. The cSH3 domain concentration was determined by UV absorption ($\lambda = 280$), $\epsilon = 8370\ M^{-1}\ cm^{-1}$. The final yield of the purified cSH3 domain was ~3 mg/L.

NMR Spectroscopy. All NMR experiments were recorded at 25 °C using Bruker Avance 500, 600, 700, and 800 MHz spectrometers (equipped with CryoProbes) and Varian Inova 600 spectrometers, equipped with triple-resonance probes. All NMR data were processed using NMRpipe and visualized using NMRDraw (*32*). NMRView was used to analyze all NMR data (*33*). ^{1}H chemical shifts were referenced to water at 4.75 ppm (at 25 °C), whereas the $\gamma^{13}C/\gamma^1H$ and $\gamma^{15}N/\gamma^1H$ ratios were used for indirect referencing of the ^{13}C and ^{15}N chemical shifts. ^{1}H-^{15}N heteronuclear single-quantum coherence (HSQC), ^{1}H-^{13}C HSQC, 3D-^{15}N nuclear Overhauser effect spectrometry (NOESY)−HSQC, HNCO, HNCACB, and CBCA(CO)NH experiments were used to obtain the sequential assignment of the backbone (*34*). Side-chain carbon and proton assignments were obtained using C(CO)-NH, HC(CO)NH, HBHA(CO)NH, and HCCH total correlation spectroscopy (TOCSY) experiments. To assign the aromatic resonances, ^{1}H{^{13}C} HSQC, (Hβ)Cβ(CγCδ)Hδ and (Hβ)Cβ(CγCδCϵ)Hϵ (*35*), and 3D ^{1}H{^{13}C} NOESY−HSQC data were utilized.

Backbone ^{15}N Relaxation Measurements and Analysis. A complete set of backbone amide R_1, R_2, and ^{15}N{^{1}H} nuclear Overhauser effect (NOE) relaxation data sets were acquired on Bruker 700 and 800 MHz machines using the pulse sequence published previously (*36*). The R_1 and R_2 data sets were collected at 25 °C using a recycle delay of 1.5 s. The R_1 measurements were obtained using the following variable relaxation delays: 20, 40 (×2), 60, 90, 210, 390, 560, and 710 ms, on both 700 and 800 MHz spectrometers. For the R_2 measurements, the following relaxation delays 0 (×2), 16.9, 33.9, 67.9, 84.9, 101.8, 118.8, 135.8, and 169.8 ms were used on both the 700 and 800 MHz spectrometers. The steady-state ^{15}N{^{1}H} NOE relaxation data were recorded with and without the proton saturation of 3.0 s in an interleaved experiment. The error estimation was done using duplicate data sets. The relaxation rates R_1 and R_2 were determined by fitting the experimental data to a single-exponential function using CURVEFIT (A. G. Palmer III, Columbia University, New York).

Dihedral Angle, Distance, Hydrogen-Bond Restraints, and Structure Calculations. The backbone dihedral angles (ϕ and ψ) were calculated by analyzing the $^{13}C_\alpha$, $^{13}C_\beta$, $^{13}C'$, and ^{15}N chemical shifts with the TALOS program that predicts the backbone torsion angles from the amino acid sequence and chemical-shift information (*37*). The dihedral angle ϕ was also obtained from the HNHA experiment (*38*). Hydrogen-bond restraints were obtained from 2D ^{3}J-HNCO (*39*). Inter-β-strand NOEs were also observed for these hydrogen bonds. During later stages of structure calculations, these hydrogen bonds were added as explicit restraints. The hydrogen-bonding restraints were defined as 1.8−2.3 Å for the H−O distance and 2.8−3.3 Å for the N−O distance.

Distance restraints were derived from 3D ^{13}C-edited NOESY (150 ms mixing time) and 3D ^{15}N-edited NOESY (150 ms mixing time) experiments. Using NMRView, the NOESY cross-peak volumes/intensities were obtained and converted into distance restraints using the ambiguous distance restraints (ADRs) protocol within the ARIA program (*40*, *41*). Structure calculations were performed using the Cartesian dynamics simulated annealing protocol within ARIA/CNS. The following refinement protocol was used: a high-temperature dynamics of 2000 K (10 000 steps), followed by a Cartesian dynamics cooling stage from 2000 to 1000 K (6000 steps), which was followed by a second cooling stage from 1000 to 50 K (4000 steps). In the final structure calculation run, 500 structures were calculated and 40 lowest energy structures were further refined in water using the protocol described by Linge et al. (*42*). The NMR structures were displayed and analyzed using MOLMOL (*43*), PROCHECK (*44*), WHAT IF (*45*), and SwissPDB Viewer (*46*). The electrostatic potentials were calculated using SwissPDB Viewer and GRASP (*47*). The hydrophobic core residue surface areas were calculated using MOLMOL (*43*).

Equilibrium Unfolding Measurements. The urea denaturation experiments were performed on a Spex Fluorolog-3 spectrofluorimeter at 25 °C using a 1 cm path-length cuvette with constant stirring. The excitation and emission wavelengths were 295 and 340 nm, respectively. The signal was averaged for 60 s at each urea concentration after 5 min of incubation. The concentration of urea was determined by refractometry. The protein concentration was 5 μM in 20 mM sodium phosphate (pH 7.2) and 50 mM NaCl. The fluorescence signals at each urea concentration were fit to the equation (*48*)

$$F_{\mathrm{Urea}} = \left\{\frac{\alpha_N + \beta_N[\mathrm{Urea}] + (\alpha_D + \beta_D[\mathrm{Urea}])e^{-\Delta G_u([\mathrm{Urea}])/RT}}{1 + e^{-\Delta G_u([\mathrm{Urea}])/RT}}\right\} \quad (1)$$

where

$$\Delta G_u[\mathrm{Urea}] = \Delta G^0_{H_2O} - m[\mathrm{Urea}] \quad (2)$$

and F_{Urea} is the measured fluorescence signal. α_N, β_N, α_D, and β_D are parameters defining the fluorescence signals of the native state (N) and the denatured state (D) as a function of the urea concentration. $\Delta G^0_{H_2O}$ is the Gibb's free energy of unfolding in the absence of urea. Using F_{urea}, α_N, β_N, α_D, and β_D, we determined the fraction of protein folded at a given urea concentration.

Stopped-Flow Measurements. Stopped-flow fluorescence measurements were performed using an Applied Photophys-

ics SX.18MV stopped-flow reaction analyzer equipped for asymmetric mixing at a ratio of 10:1. Fluorescence measurements were made with an excitation wavelength of 279 nm using a 305 nm cutoff filter. The refolding and unfolding reactions were initiated by 11-fold dilution. All solutions contained 10 mM sodium phosphate buffer (pH 7.3) and 50 mM sodium chloride. The temperature of the syringes and flow cell was maintained at 25 °C with a circulating water bath. The resulting curves were fitted with a single exponential to determine rate constants for each reaction. The plots of ln k_{obs} versus the denaturant concentration were fit to the following equation to determine the folding and unfolding rate constants in the absence of the denaturant, $k_f(H_2O)$ and $k_u(H_2O)$:

$$\ln(k_{obs}) = \ln\left\{k_f(H_2O)e^{\frac{m_f[Urea]}{RT}} + k_u(H_2O)e^{\frac{m_u[Urea]}{RT}}\right\} \quad (3)$$

where m_f and m_u are constants that describe the change in ln k_f and ln k_u as a function of the concentration of urea.

RESULTS

Solution Structure of the Crk-II cSH3 Domain. Sequence homology suggests that the cSH3 domain of Crk-II extends from P237 to L294 (Figure 1). However, sequence alignment analysis lacks the ability to predict domain boundaries with absolute certainty. Indeed, in the case of the nSH3 domain of Crk-II, minor truncations at the N terminus can have serious consequences on the folding of the domain (*20*). Therefore, a slightly longer cSH3 domain construct was used in our studies, extending from L230 to S304. An initial estimate of the rotational diffusion tensor was made using the ^{15}N relaxation rates R_1 and R_2 and $^{15}N\{^1H\}$ NOE values after removing the overlapping residues and those that had potential chemical-exchange contributions. The best model that fits the NMR data (data not shown) was an isotropic model with the overall correlation time (τ_c) of 5.27 ns. This strongly suggests that the cSH3 domain behaves as a monomer in solution.

The uniformly ^{15}N- and ^{13}C-labeled cSH3 domain was used to obtain the main- and side-chain assignments of the ^1H, ^{15}N, and ^{13}C resonances using the standard set of triple-resonance 3D experiments (*49*) (Table S1 in the Supporting Information). All backbone assignments were made with the exception of the amide nitrogen and amide proton resonances of L230, V247, and V271 (Figure 2A). There are five proline residues in the cSH3 domain, and they are in trans configuration based on H_α-H_δ/H_δ' NOE data.

An initial assessment of the cSH3 secondary structure was made using the deviations of assigned chemical shifts from random coil (*50*). This indicates that the domain consists of five β strands as seen for other SH3 domains. The steady-state $^{15}N\{^1H\}$ heteronuclear Overhauser effect (NOE) (Figure 2B) indicates that, except for residues at the N terminus (L230−G236) and C terminus (L294−S304), the domain is well-ordered with relatively little flexibility in the intervening sequence compared to the termini of the domain. Therefore, residues L230−N235 at the N terminus and residues P299−S304 at the C terminus were excluded from the final structure calculation.

All NOE cross-peaks in the ^{15}N NOESY−HSQC and ^{13}C NOESY−HSQC spectra were used by ARIA/CNS. The final

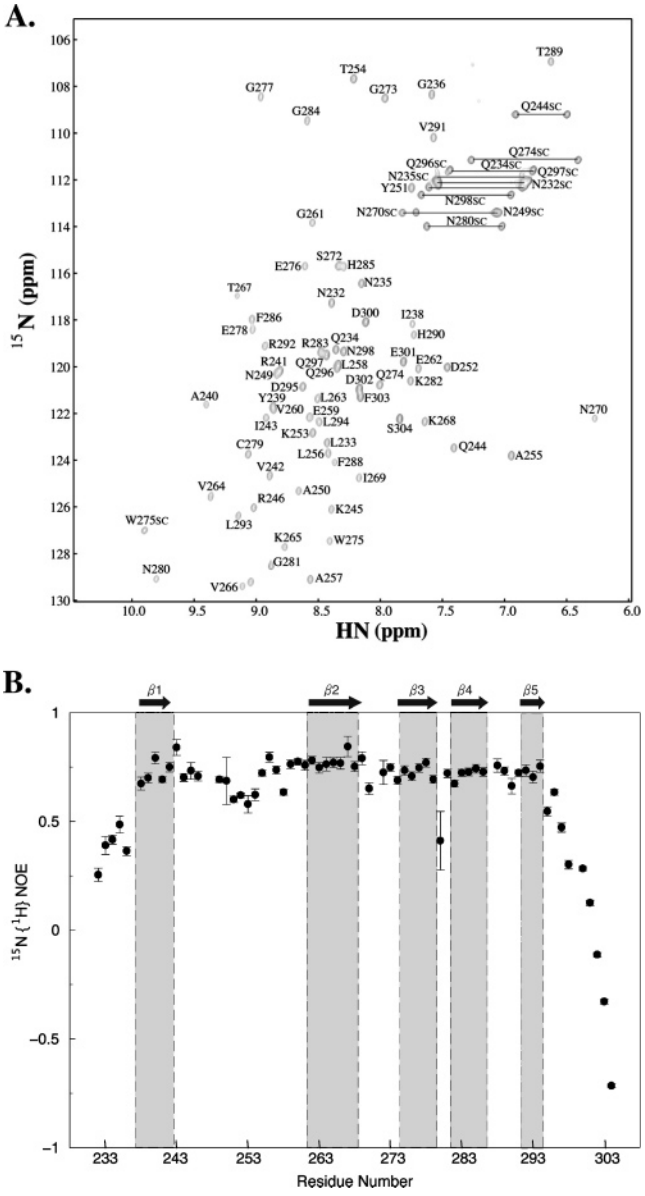

FIGURE 2: NMR analysis of the cSH3 domain. (A) Assigned ^1H-^{15}N HSQC spectrum of the cSH3 domain. (B) $^{15}N\{^1H\}$ heteronuclear NOE measurements for the cSH3 domain. Residues that have NOE values of 0.7 or more are expected to be well-ordered, and those with NOE values of less than 0.7 are expected to be in flexible loops or linker regions.

set of structure calculations were performed using a total of 1074 unambiguous restraints (538 intraresidue, 238 sequential, 91 short range, 17 medium range, and 190 long range). Furthermore, 291 ambiguous restraints were also incorporated in the structure calculations. In addition, 96 dihedral (49 ϕ and 47 ψ) and 46 hydrogen-bond restraints were used in the structure calculations. There was no increase of the target function upon adding the hydrogen-bond restraints. Structural statistics and analysis are given in Table 1.

The 20 lowest energy structures are superimposed in Figure 3A (PDB code 2GGR). These structures exhibit no distance and dihedral restraint violations greater than 0.5 Å and 5°, respectively. The structure ensemble has an average pairwise atomic root-mean-square deviation (rmsd) of 0.68 ± 0.17 Å for backbone residues and 1.39 ± 0.21 Å for heavy-atom residues. The rmsd of the ensemble with respect to the average structure was 0.48 ± 0.12 Å for the main

Table 1: NMR Restraints and Structural Statistics for the Best 20 Structures

restraints and statistics	
total number of restraints	1507
NOE restraints	1365
unambiguous	1074
intraresidue	538
sequential	238
short range	91
medium range	17
long range	190
ambiguous	291
dihedral-angle restraints	96
hydrogen-bond restraints	46
structure statistics	
NOE violations > 0.5 Å	0
dihedral violations > 5°	0
total energy (kcal/mol)	-2007 ± 57
NOE constraints energy (kcal/mol)	147 ± 25
rmsd from average structure	
backbone (N, Cα, C) (Å)	0.48 ± 0.12
heavy atoms (Å)	0.99 ± 0.12
Ramachandran statistics	
most favored region (%)	74.8
additionally allowed (%)	24.6
generously allowed (%)	0.6
disallowed (%)	0.0

chain and 0.99 ± 0.12 Å for the heavy atoms. The quality of the structures were analyzed using PROCHECK and WHATIF (Table 1). The three-dimensional structure of the Crk-II cSH3 domain has five β strands (residues $\beta1$ = I238−V242, $\beta2$ = E262−K268, $\beta3$ = W275−C279, $\beta4$ = K282−F286, and $\beta5$ = R292−L294) organized in an antiparallel β-barrel structure (Figure 3B). The secondary structure of the cSH3 domain is similar to that determined by homology modeling (*51*). Analogous to all other SH3 domains, the stands are connected by a series of loops, namely, residues I243−G261 (by convention the RT loop), residues I269−Q274 (the nSrc loop), and residues N280−G281 (the distal loop). The last two β strands are connected by a short 3_{10} helix from F288 to H290.

The cSH3 domain adopts the canonical SH3 domain fold. For example, the backbone rmsd of the cSH3 domain obtained after structural alignment to the nSH3 domain (1cka) of Crk-II is 1.29 Å (Figure S2 in the Supporting Information). The cSH3 domain possesses a compact hydrophobic core comprising several residues that collectively bury 2249 Å^2 of residue surface area, which is similar to that seen in other SH3 domains (e.g., nSH3 = 2355 Å^2). The hydrophobic core also includes L256, L258, V264, and V266, which are a part of the putative NES in the cSH3 domain (*31*) (Figure 4A). Noteworthy is the presence of the valine residue at position 242, within the first β strand. The corresponding residue in other SH3 domains is ~75% conserved as Ala (*30*) (Figure 1). The extra volume associated with having the branched valine residue in the core seems to be accommodated, at least in part, by the presence of A240, whose position is usually a slightly larger hydrophobic residue in other SH3 domains. This reorganization underscores the plasticity of the hydrophobic core of SH3 domains (*52*).

The ligand-binding surface of SH3 domains is characterized by several conserved aromatic residues (Figure 1). Most of these conserved residues are mutated to more polar, nonaromatic residues in the cSH3 domain, specifically, Q244, R246, Q274, and H290 (Figure 4B). Thus, a question at the outset of this study was whether the conserved aromatic residues on the ligand-binding surface have been replaced with nonconserved aromatic residues or is the surface indeed more polar? On the basis of structural alignment of the cSH3 and the nSH3 domains, the residues that form a canonical ligand-binding pocket in the cSH3 domain are Q244, G273, Q274, P287, T289, and H290. These residues are exposed to the bulk solvent in the structure forming a contiguous surface on the cSH3 domain that corresponds to the ligand-binding surface on most other SH3 domains (Figure 4B). Some of these residues also contribute to make the surface

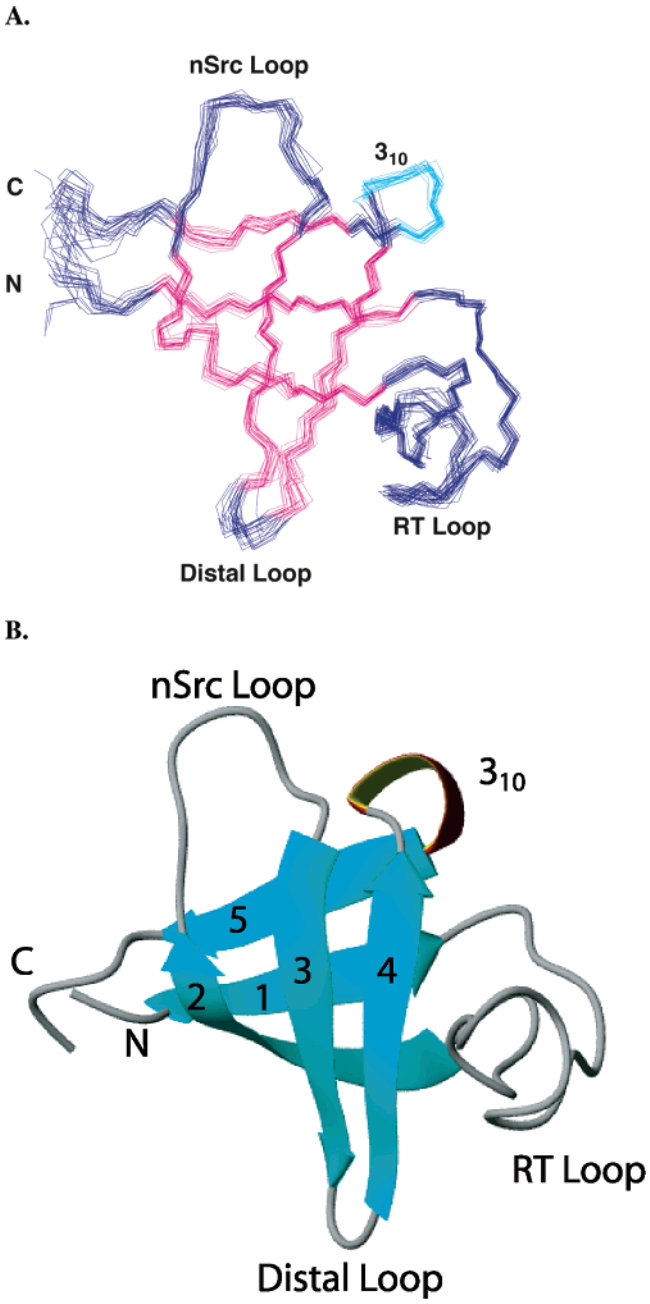

FIGURE 3: Solution structure of the cSH3 domain of Crk-II (PDB code 2GGR). The structures were drawn using MOLMOL (*43*). (A) The main chain of the 20 lowest energy structures are superimposed. β strands are shown in red; loops are shown in blue; and the 3_{10} helix is shown in cyan. (B) Ribbon diagram of the cSH3 domain.

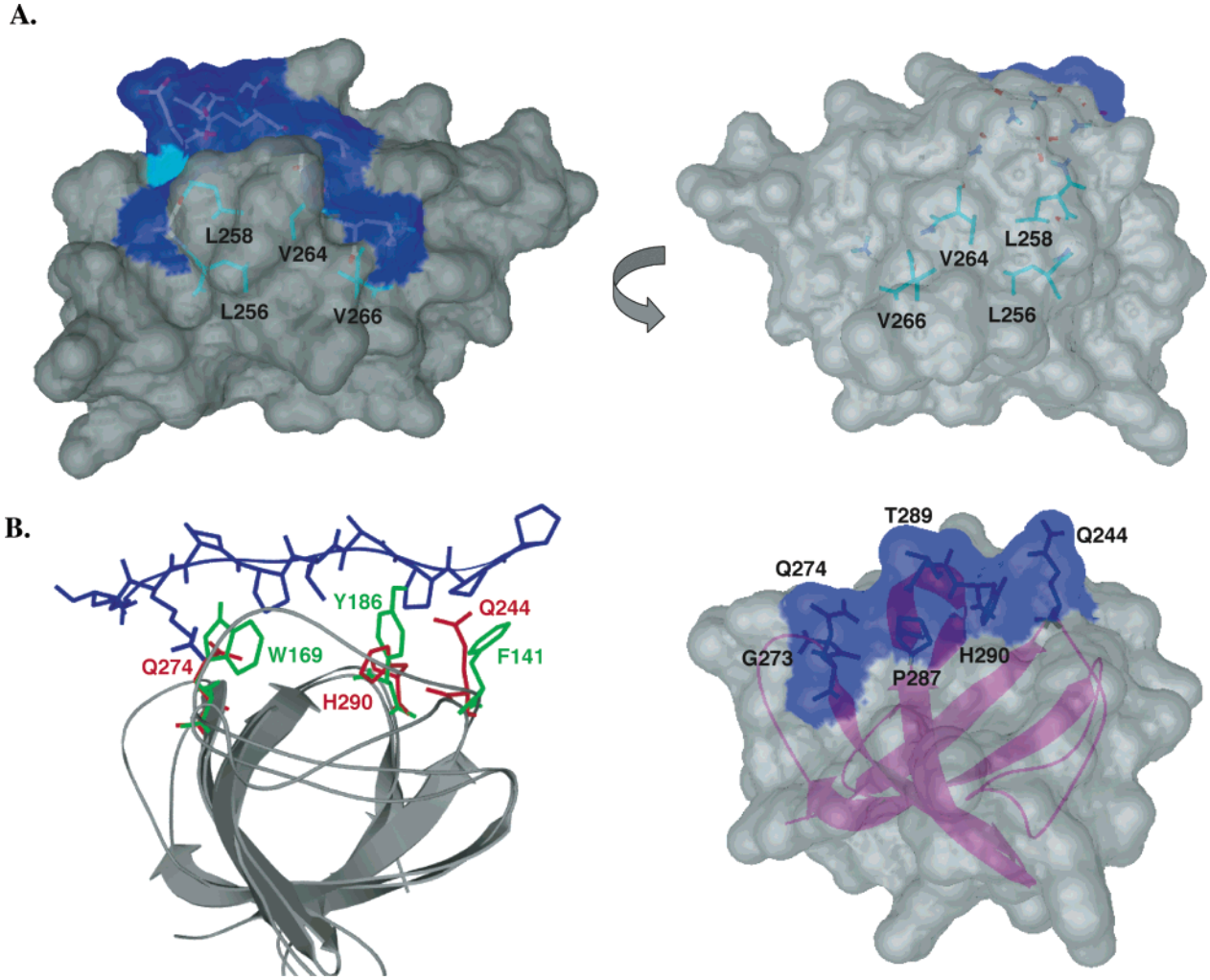

FIGURE 4: Structure of the cSH3 domain. (A) Surface representation of the putative NES (highlighted in blue and cyan) in the cSH3 domain. The residues in cyan are part of the hydrophobic core of the domain and are indicated. (B) Overlaid structures of the nSH3 and cSH3 domains of Crk-II are shown (left). The polyproline ligand for the nSH3 domain is also shown (in blue). The aromatic residues that line the ligand-binding pocket in the nSH3 domain (in green) and the corresponding residues occupying the same position in the cSH3 domain (in red) are also indicated. The residues that form the entire canonical ligand-binding pocket in the cSH3 domain are shown in a surface representation and are indicated (right).

of the cSH3 domain basic in nature (Figure 5). The functional significance of this surface-charge distribution is unclear.

Folding Properties of the cSH3 Domain of Crk-II. The change in the fluorescence signal of the tryptophan residue upon the addition of chemical denaturants was used to determine the equilibrium stability of the cSH3 domain. The structure shows that this tryptophan residue is buried in the hydrophobic core of the cSH3 domain. The tryptophan packs against several residues (I238, V266, F288, V291, and L293) and results in the burial of 1117 Å^2 of the hydrophobic surface area. The unfolding of the cSH3 domain exposes this buried tryptophan to the bulk solvent. This results in a substantial change in the fluorescence intensity upon the addition of chemical denaturation, a 3-fold decrease at 340 nm. The domain exhibited a well-defined unfolding curve from which we elucidated the stability ($\Delta G^0_{H_2O}$) and *m* value for the cSH3 domain using eq 1 (Figure 6A and Table 2).

Equilibrium denaturation measurements show that the cSH3 domain folds in a reversible apparent two-state manner. The equilibrium stability of the cSH3 domain was found to be 3.3 kcal mol^{-1}, which is similar to that observed for other SH3 domains (*20*, *53*−*56*) (Table 2). The *m* value, which is proportional to the change in the solvent-exposed surface area upon unfolding, is 0.66 kcal mol^{-1} M^{-1}, which is slightly lower than that seen for other SH3 domains (*20*, *56*) (Table 2).

The folding kinetics of the cSH3 domain was measured using fluorescence-detected stopped-flow experiments. Interestingly, the data can be fit to a single-exponential decay; i.e., the refolding of the cSH3 domain is monophasic. This was surprising because the cSH3 domain contains five proline residues, which was expected to result in a slow phase in the folding amplitude because of proline cis−trans isomerization as observed in most other SH3 domains (*20*, *54*−*56*). One explanation for this is that the population of *cis*-prolyl peptide bonds in the unfolded state is below the detection limit of the stopped-flow instrument. Alternatively, the proline isomerization could occur after the rate-determining step as detected by Trp fluorescence. Note, Pro287 is closest (~5 Å) to the Trp in the structure. This situation is reminiscent of the Fyn SH3 domain, which also exhibits

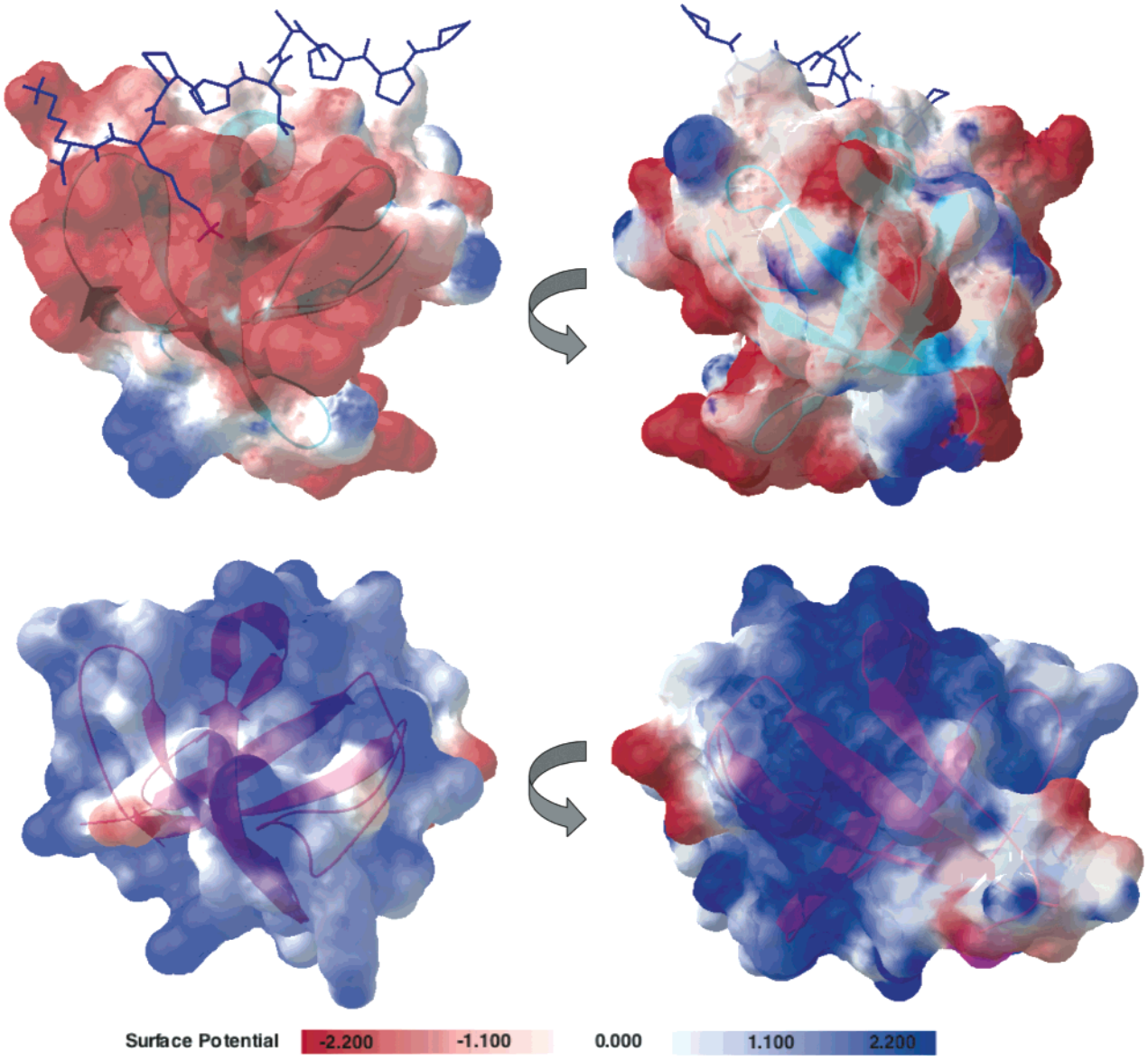

FIGURE 5: Surface representation of the nSH3 (top, 1cka) and cSH3 (bottom) domains, showing the surface-charge distribution on the two domains. The electrostatic surface representation of the two structures was drawn using SwissPDB Viewer (*46*). The polyproline ligand is shown for the nSH3 domain.

monophasic refolding behavior despite containing two proline residues that are trans in the native state (*53*). Figure 6B shows the plot of the natural logarithm of the observed rate constant, k_{obs}, versus the urea concentration. The chevron plots show a classic V-shape curve, as expected for a protein that folds in a two-state manner. From this, we elucidated the folding rate (k_f) of the cSH3 domain to be 82.6 s^{-1} and the unfolding rate (k_u) to be 0.17 s^{-1} (Table 2). At low denaturation concentrations, we did not observe any rollover, i.e., deviation from linearity. The $\Delta G°$ and m values calculated from the kinetic measurements, 3.66 kcal mol^{-1} and 0.71 kcal mol^{-1} M^{-1}, are in good agreement with the equilibrium measurements (Table 2). The ratio of m_f/m_{total}, denoted β_T, is a measure of the relative compactness of the transition state. The calculated value for cSH3 is 0.79, indicating a compact transition-state ensemble. This value is similar to that observed for other SH3 domains. For example, the value for the nSH3 domain of Crk-II is 0.71 (*20*). The kinetic data is also consistent with an apparent two-state folding model.

DISCUSSION

SH3 domains are small (~60 residues) protein−protein interaction domains. They have been found within approximately 1000 proteins from organisms ranging from yeast to humans (*57*). The sequence identity between different SH3 domains is low, ranging from 15 to 45%, with the average pairwise identity being around 27% (*30*). Despite this, all SH3 domains fold in a similar manner to adopt a five-stranded β-barrel structure (currently 380 structures in the PDB). This incongruity (i.e., low sequence homology versus high structural homology) has made SH3 domains an important model system for protein-folding studies (*53*−*56*). In the present work, we have found that the cSH3 domain of Crk-II also folds with a five-stranded β-barrel structure (Figure 3B). In addition, the thermodynamic

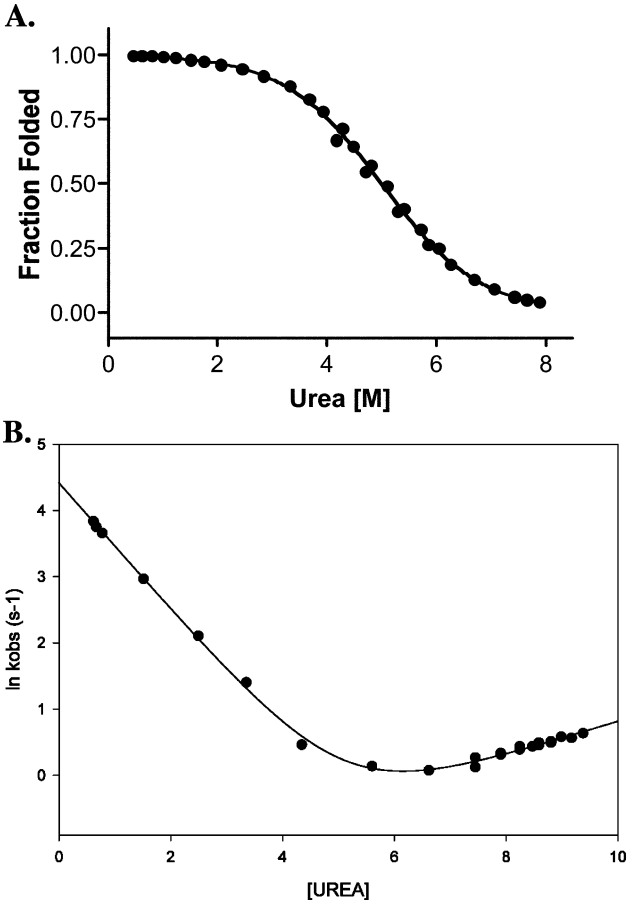

FIGURE 6: Folding properties of the cSH3 domain. (A) Equilibrium denaturation of the cSH3 domain. The fluorescence intensity was recorded as a function of the urea concentration. The solid line represents the best fit to eqs 1 and 2. (B) Chevron plot of the natural logarithm of the observed rate constant as a function of the urea concentration. The solid line represents the best fit to eq 3.

Table 2: Folding Thermodynamics and Kinetics for the cSH3 Domain[a]

equilibrium thermodynamics	
$\Delta G^0_{H_2O}$ (kcal mol^{-1})	3.33 ± 0.3
m value (kcal mol^{-1} M^{-1})	0.66 ± 0.1
folding kinetics	
k_f (s^{-1})	82.6 ± 2.9
k_u (s^{-1})	0.17 ± 0.03
ΔG^0_{kin} (kcal mol^{-1})	3.66
m_f value (kcal mol^{-1} M^{-1})	0.57 ± 0.01
m_u value (kcal mol^{-1} M^{-1})	0.15 ± 0.01
m_{tot} value (kcal mol^{-1} M^{-1})	0.72

[a] All experiments were performed at 25 °C in 20 mM sodium phosphate and 100 mM sodium chloride at pH 7.2. The numbers following the ± represent standard errors to the fit.

stability and kinetic folding properties of the cSH3 domain are comparable to other SH3 domains.

Despite the low sequence conservation, the majority of the SH3 domains bind to proline-rich sequences (PXXP) via key conserved aromatic residues that form a contiguous hydrophobic patch on the surface of the protein. Burial of these hydrophobic residues accounts for the moderately high affinity (usually low micromolar) associated with the PXXP-binding interaction; ligand binding typically results in the burial of 800−1200 Å^2 of surface area, most of which is hydrophobic in nature (*58*, *59*). The specificity of ligand binding arises out of ancillary interactions usually involving polar or charged residues flanking the core PXXP sequence (*19*, *58*). In contrast, these conserved hydrophobic residues are replaced by polar residues in the cSH3 domain (Figure 1). Indeed, our structure shows that these residues form a continuous surface that corresponds to the ligand-binding surface on other SH3 domains (Figure 4B). Consequently, the energy derived from the burial of hydrophobic residues upon ligand binding (*60*) is no longer available in the case of the cSH3 domain. This suggests that the cSH3 domain probably does not bind to PXXP sequences with high affinity, assuming that the interaction is canonical. It is also possible that the domain binds to other sequences, as observed in several SH3 domains including the Pix SH3 domain (*61*), the Eps8 SH3 domain (*62*), the Gads SH3 domain (*63*), and the Hbp SH3 domain (*64*). However, we note that the conserved hydrophobic residues involved in ligand binding are also present in these SH3 domains. It is therefore unsurprising that efforts to find a PXXP ligand for this domain have not yet been fruitful (*5*).

The only known interaction involving the cSH3 domain is with the nuclear export factor, Crm1 (*31*). Affinity pull-down assays indicate that the Crk-II−Crm1 interaction is dependent upon a putative NES within the cSH3 domain (L256−V266). Several residues in this sequence are part of the hydrophobic core of the domain, namely, L256, L258, V264, and V266 (Figure 4A). Recognition of this NES by Crm1 would therefore require unfolding of the cSH3 domain to expose the sequence. We determined the free energy of unfolding ($\Delta G^0_{H_2O}$) of the cSH3 domain to be 3.66 kcal mol^{-1} (Figure 6). On the basis of this equilibrium stability, Crm1 would have to bind to the NES with low nanomolar affinity to compensate for the free-energy loss associated within unfolding the domain. Crm1 is thought to bind NES-containing cargoes and RanGTP in a cooperative manner with affinities in the nanomolar range (*65*). Thus, there could be enough binding energy associated with a Crm1−RanGTP−Crk ternary complex to maintain the cSH3 domain in an unfolded state (*65*). This is an intriguing idea, and there are certainly examples of binding events that maintain proteins in the unfolded or partially folded state (*66*, *67*). At the same time, it is worth considering the possibility that Crm1 actually binds to the surface of the folded cSH3 domain. Indeed, the principle line of evidence for the involvement of an NES in the CRM1−cSH3 interaction comes from the inability of Crm1 to bind a cSH3 mutant in which residues 263, 264, 266 are replaced with alanine. As noted above, V264 and V266 are part of the hydrophobic core of the protein, and thus, the native fold of this triple mutant would be expected to be dramatically destabilized. Consequently, any binding interaction requiring the native SH3 fold would also be weakened. Although Crm1 does not contain any PXXP motifs, there are several examples of SH3 domains that bind to noncanonical ligands (*61*, *62*, *64*), and given the unusual nature of the binding pocket in cSH3, such a possibility cannot be discounted in this case. Clearly, further biochemical and structural analysis of the Crm1−cSH3 interaction is merited.

A recent study also alludes to the possibility that the cSH3 domain might be involved in the activation of the Abl kinase by Crk-II (*51*). Abl kinase is known to interact with both the SH2 and nSH3 domains of Crk-II (*17*, *18*, *24*). The

authors of this study have identified a conserved sequence in the RT loop of the cSH3 domain ($P^{248}NAY^{251}$) that might play a role in the activation of Abl kinase (*51*). However, deletion of this sequence alone does not have an effect on Abl kinase activation (*51*). Only when combined with other mutations in Crk-II does the deletion of the PNAY sequence show an inhibitory effect on Abl kinase (*51*). In the structure of the cSH3 domain, the PNAY sequence points into solution and therefore is available for potential interactions. Several recent studies have shown that mutating the single tryptophan residue in the cSH3 domain can lead to the disruption of the normal function of Crk-II (*27*, *28*). This tryptophan is an integral part of the hydrophobic core of the domain. The fluorescence of this tryptophan residue shows a robust decrease upon the addition of denaturants, which allowed us to follow the folding of this domain. We also replaced the tryptophan residue with 7-azatryptophan using *E. coli* Trp auxotrophic cells (*21*), which destabilized the cSH3 domain by ~1 kcal mol^{-1}, about a 25% decrease in the overall free energy of folding (data not shown). This strongly suggests that mutation of the tryptophan residue results in the unfolding of the domain, which leads to the observed deregulation of the function of Crk-II (*27*, *28*).

Several lines of evidence indicate that the cSH3 domain acts to negatively regulate the function of Crk-II. Specifically, mutations that disrupt the structure of the cSH3 domain interfere with the regulation of Crk-II leading to an abrogation of phagocytosis (*27*) and endocytosis (*28*). The mechanism by which the cSH3 domain regulates the Crk function is unknown. There are no known PXXP-type binding partners for this domain, despite considerable efforts to identify such ligands (*5*). As a consequence, several groups have speculated on the possibility of intrasteric regulation (*5*, *26*). In this scheme, the cSH3 domain would participate in an intramolecular interaction with another region of the protein, perhaps involving the proline-rich sequences within either the SH2 domain or the extended linker between the two SH3 domains. Several SH3 domains are known to bind ligands in an intramolecular fashion (*68*−*70*), and one of the factors governing self-association is the affinity of the SH3 domain for the ligand; lower affinities have been shown to favor intramolecular-binding events (*71*). Thus, it is intriguing to note that the canonical ligand-binding surface of the cSH3 domain is atypical, being much less hydrophobic and hence likely to lead to reduced affinity for PXXP sequences (Figure 4B). An unexpected feature of the cSH3 domain was the basic nature of its surface (Figure 5). Interestingly, the nSH3 domain of Crk-II has an acidic surface (Figure 5). Such a distribution of charges has not been seen in proteins with multiple SH3 domains for which structures are available (*70*, *72*, *73*). This raises the question of whether the nSH3 and cSH3 domains of Crk-II associate through electrostatic interactions? Ultimately, the role of the cSH3 domain in Crk-II regulation will be best addressed by high-resolution structural analysis on the full-length protein. The availability of the structural and thermodynamic data generated in the present study will be helpful in this regard.

ACKNOWLEDGMENT

We thank Dr. Michael Goger for helpful suggestions and discussion on the NMR spectroscopy.

SUPPORTING INFORMATION AVAILABLE

Figure S1, RP-HPLC and ESMS characterization of the purified, uniformly ^{13}C- and ^{15}N-labeled cSH3 domain; Figure S2, structural alignment of the cSH3 domain with other SH3 domains; Table S1, chemical-shift assignments of the cSH3 domain. This material is available free of charge via the Internet at http:// pubs.acs.org.

REFERENCES

1. Lamorte, L., Royal, I., Naujokas, M., and Park, M. (2002) Crk adapter proteins promote an epithelial-mesenchymal-like transition and are required for HGF-mediated cell spreading and breakdown of epithelial adherens junctions, *Mol. Biol. Cell 13*, 1449−1461.
2. Lamorte, L., Rodrigues, S., Naujokas, M., and Park, M. (2002) Crk synergizes with epidermal growth factor for epithelial invasion and morphogenesis and is required for the Met morphogenic program, *J. Biol. Chem. 277*, 37904−37911.
3. Abassi, Y. A., and Vuori, K. (2002) Tyrosine 221 in Crk regulates adhesion-dependent membrane localization of Crk and Rac and activation of Rac signaling, *EMBO J. 21*, 4571−4582.
4. Zvara, A., Fajardo, J. E., Escalante, M., Cotton, G., Muir, T., Kirsch, K. H., and Birge, R. B. (2001) Activation of the focal adhesion kinase signaling pathway by structural alterations in the carboxyl-terminal region of c-Crk II, *Oncogene 20*, 951−961.
5. Feller, S. M. (2001) Crk family adaptors−Signalling complex formation and biological roles, *Oncogene 20*, 6348−6371.
6. Reddien, P. W., and Horvitz, H. R. (2000) CED-2/CrkII and CED-10/Rac control phagocytosis and cell migration in *Caenorhabditis elegans*, *Nat. Cell Biol. 2*, 131−136.
7. KizakaKondoh, S., Matsuda, M., and Okayama, H. (1996) CrkII signals from epidermal growth factor receptor to Ras, *Proc. Natl. Acad. Sci. U.S.A. 93*, 12177−12182.
8. Hasegawa, H., Kiyokawa, E., Tanaka, S., Nagashima, K., Gotoh, N., Shibuya, M., Kurata, T., and Matsuda, M. (1996) DOCK180, a major CRK-binding protein, alters cell morphology upon translocation to the cell membrane, *Mol. Cell Biol. 16*, 1770−1776.
9. Reichman, C. T., Mayer, B. J., Keshav, S., and Hanafusa, H. (1992) The product of the cellular Crk gene consists primarily of Sh2 and Sh3 regions, *Cell Growth Differ. 3*, 451−460.
10. Matsuda, M., Tanaka, S., Nagata, S., Kojima, A., Kurata, T., and Shibuya, M. (1992) Two species of human CRK cDNA encode proteins with distinct biological activities, *Mol. Cell Biol. 12*, 3482−3489.
11. ten Hoeve, J., Morris, C., Heisterkamp, N., and Groffen, J. (1993) Isolation and chromosomal localization of CRKL, a human crk-like gene, *Oncogene 8*, 2469−2474.
12. Schaller, M. D., and Parsons, J. T. (1995) pp125FAK-dependent Tyrosine phosphorylation of paxillin creates a high-affinity binding site for Crk, *Mol. Cell Biol. 15*, 2635−2645.
13. Nojima, Y., Morino, N., Mimura, T., Hamasaki, K., Furuya, H., Sakai, R., Sato, T., Tachibana, K., Morimoto, C., Yazaki, Y., et al. (1995) Integrin-mediated cell adhesion promotes tyrosine phosphorylation of p130Cas, a Src homology 3-containing molecule having multiple Src homology 2-binding motifs, *J. Biol. Chem. 270*, 15398−15402.
14. de Jong, R., Haataja, L., Voncken, J. W., Heisterkamp, N., and Groffen, J. (1995) Tyrosine phosphorylation of murine Crkl, *Oncogene 11*, 1469−1474.
15. Feller, S. M., Knudsen, B., and Hanafusa, H. (1994) C-Abl kinase regulates the protein-binding activity of c-Crk, *EMBO J. 13*, 2341−2351.
16. Rosen, M. K., Yamazaki, T., Gish, G. D., Kay, C. M., Pawson, T., and Kay, L. E. (1995) Direct demonstration of an intramolecular SH2−phosphotyrosine interaction in the Crk protein, *Nature 374*, 477−479.
17. Anafi, M., Rosen, M. K., Gish, G. D., Kay, L. E., and Pawson, T. (1996) A potential SH3 domain-binding site in the Crk SH2 domain, *J. Biol. Chem. 271*, 21365−21374.
18. Donaldson, L. W., Gish, G., Pawson, T., Kay, L. E., and Forman-Kay, J. D. (2002) Structure of a regulatory complex involving the Abl SH3 domain, the Crk SH2 domain, and a Crk-derived phosphopeptide, *Proc. Natl. Acad. Sci. U.S.A. 99*, 14053−14058.

19. Wu, X., Knudsen, B., Feller, Stephan M., Zheng, J., Sali, A., Cowburn, D., Hanafusa, H., Kuriyan, J. (1995) Structural basis for the specific interaction of lysine-containing proline-rich peptides with the N-terminal SH3 domain of c-Crk, *Structure 3*, 215−226.
20. Camarero, J. A., Fushman, D., Sato, S., Giriat, I., Cowburn, D., Raleigh, D. P., and Muir, T. W. (2001) Rescuing a destabilized protein fold through backbone cyclization, *J. Mol. Biol. 308*, 1045−1062.
21. Muralidharan, V., Cho, J. H., Trester-Zedlitz, M., Kowalik, L., Chait, B. T., Raleigh, D. P., and Muir, T. W. (2004) Domain-specific incorporation of noninvasive optical probes into recombinant proteins, *J. Am. Chem. Soc. 126*, 14004−14012.
22. Knudsen, B. S., Feller, S. M., and Hanafusa, H. (1994) 4 proline-rich sequences of the guanine-nucleotide exchange factor C3G bind with unique specificity to the first Src homology-3 domain of Crk, *J. Biol. Chem. 269*, 32781−32787.
23. Matsuda, M., Ota, S., Tanimura, R., Nakamura, H., Matuoka, K., Takenawa, T., Nagashima, K., and Kurata, T. (1996) Interaction between the amino-terminal SH3 domain of CRK and its natural target proteins, *J. Biol. Chem. 271*, 14468−14472.
24. Ren, R., Ye, Z. S., and Baltimore, D. (1994) Abl protein-tyrosine kinase selects the Crk adapter as a substrate using SH3-binding sites, *Genes Dev. 8*, 783−795.
25. Hashimoto, Y., Katayama, H., Kiyokawa, E., Ota, S., Kurata, T., Gotoh, N., Otsuka, N., Shibata, M., and Matsuda, M. (1998) Phosphorylation of CrkII adaptor protein at tyrosine 221 by epidermal growth factor receptor, *J. Biol. Chem. 273*, 17186−17191.
26. Ogawa, S., Toyoshima, H., Kozutsumi, H., Hagiwara, K., Sakai, R., Tanaka, T., Hirano, N., Mano, H., Yazaki, Y., and Hirai, H. (1994) The C-terminal SH3 domain of the mouse c-Crk protein negatively regulates tyrosine-phosphorylation of Crk associated p130 in Rat 3Y1 cells, *Oncogene 9*, 1669−1678.
27. Sun, H., Shen, Y., Dokainish, H., Holgado-Madruga, M., Wong, A., and Ireton, K. (2005) Host adaptor proteins Gab1 and CrkII promote InlB-dependent entry of *Listeria* monocytogenes, *Cell. Microbiol. 7*, 443−457.
28. Akakura, S., Kar, B., Singh, S., Cho, L., Tibrewal, N., Sanokawa-Akakura, R., Reichman, C., Ravichandran, K. S., and Birge, R. B. (2005) C-Terminal SH3 domain of CrkII regulates the assembly and function of the DOCK180/ELMO Rac-GEF, *J. Cell. Physiol. 204*, 344−351.
29. Mayer, B. J., Hamaguchi, M., and Hanafusa, H. (1988) A novel viral oncogene with structural similarity to phospholipase C, *Nature 332*, 272−275.
30. Larson, S. M., and Davidson, A. R. (2000) The identification of conserved interactions within the SH3 domain by alignment of sequences and structures, *Protein Sci. 9*, 2170−2180.
31. Smith, J. J., Richardson, D. A., Kopf, J., Yoshida, M., Hollingsworth, R. E., and Kornbluth, S. (2002) Apoptotic regulation by the Crk adapter protein mediated by interactions with Wee1 and Crm1/exportin, *Mol. Cell. Biol. 22*, 1412−1423.
32. Delaglio, F., Grzesiek, S., Vuister, G. W., Zhu, G., Pfeifer, J., and Bax, A. (1995) NMRPipe: A multidimensional spectral processing system based on UNIX pipes, *J. Biomol. NMR 6*, 277−293.
33. Johnson, B. A. (2004) Using NMRView to visualize and analyze the NMR spectra of macromolecules, *Methods Mol. Biol. 278*, 313−352.
34. Sattler, M., Schleucher, J., and Griesinger, C. (1999) Heteronuclear multidimensional NMR experiments for the structure determination of proteins in solution employing pulse field gradients, *Prog. NMR Spectrosc. 34*, 93−158.
35. Yamazaki, T., Formankay, J. D., and Kay, L. E. (1993) Two-dimensional NMR experiments for correlating C-13β and H-1δ/ϵ chemical shifts of aromatic residues in ^{13}C-labeled proteins via scalar couplings, *J. Am. Chem. Soc. 115*, 11054−11055.
36. Farrow, N. A., Muhandiram, R., Singer, A. U., Pascal, S. M., Kay, C. M., Gish, G., Shoelson, S. E., Pawson, T., Forman-Kay, J. D., and Kay, L. E. (1994) Backbone dynamics of a free and a phosphopeptide-complexed Src homology 2 domain studied by ^{15}N NMR relaxation, *Biochemistry 33*, 5984−6003.
37. Cornilescu, G., Delaglio, F., and Bax, A. (1999) Protein backbone angle restraints from searching a database for chemical shift and sequence homology, *J. Biomol. NMR 13*, 289−302.
38. Kuboniwa, H., Grzesiek, S., Delaglio, F., and Bax, A. (1994) Measurement of H^N-H^α J couplings in calcium-free calmodulin using new 2D and 3D water-flip-back methods, *J. Biomol. NMR 4*, 871−878.
39. Cornilescu, G., Hu, J. S., and Bax, A. (1999) Identification of the hydrogen bonding network in a protein by scalar couplings, *J. Am. Chem. Soc. 121*, 2949−2950.
40. Habeck, M., Rieping, W., Linge, J. P., and Nilges, M. (2004) NOE assignment with ARIA 2.0: The nuts and bolts, *Methods Mol. Biol. 278*, 379−402.
41. Linge, J. P., Habeck, M., Rieping, W., and Nilges, M. (2003) ARIA: Automated NOE assignment and NMR structure calculation, *Bioinformatics 19*, 315−316.
42. Linge, J. P., Williams, M. A., Spronk, C. A., Bonvin, A. M., and Nilges, M. (2003) Refinement of protein structures in explicit solvent, *Proteins 50*, 496−506.
43. Koradi, R., Billeter, M., and Wuthrich, K. (1996) MOLMOL: A program for display and analysis of macromolecular structures, *J. Mol. Graphics 14*, 51−55, 29−32.
44. Laskowski, R. A., Rullmannn, J. A., MacArthur, M. W., Kaptein, R., and Thornton, J. M. (1996) AQUA and PROCHECK-NMR: Programs for checking the quality of protein structures solved by NMR, *J. Biomol. NMR 8*, 477−486.
45. Vriend, G. (1990) What if—A molecular modeling and drug design program, *J. Mol. Graphics 8*, 52−57.
46. Guex, N., and Peitsch, M. C. (1997) SWISS-MODEL and the Swiss-PdbViewer: An environment for comparative protein modeling, *Electrophoresis 18*, 2714−2723.
47. Nicholls, A., Sharp, K. A., and Honig, B. (1991) Protein folding and association: Insights from the interfacial and thermodynamic properties of hydrocarbons, *Proteins 11*, 281−296.
48. Pace, C. N. (1986) Determination and analysis of urea and guanidine hydrochloride denaturation curves, *Methods Enzymol. 131*, 266−280.
49. Cavanagh, J., Fairbrother, J. W., Palmer, A. G., III, and Skelton, N. J. (1996) *Protein NMR Spectroscopy; Principles and Practice*, 1st ed., Academic Press, San Diego, CA.
50. Wishart, D. S., and Sykes, B. D. (1994) The ^{13}C chemical-shift index: A simple method for the identification of protein secondary structure using ^{13}C chemical-shift data, *J. Biomol. NMR 4*, 171−180.
51. Reichman, C., Singh, K., Liu, Y., Singh, S., Li, H., Fajardo, J. E., Fiser, A., and Birge, R. B. (2005) Transactivation of Abl by the Crk II adapter protein requires a PNAY sequence in the Crk C-terminal SH3 domain, *Oncogene 24*, 8187−8199.
52. Northey, J. G., Di Nardo, A. A., and Davidson, A. R. (2002) Hydrophobic core packing in the SH3 domain folding transition state, *Nat. Struct. Biol. 9*, 126−130.
53. Plaxco, K. W., Guijarro, J. I., Morton, C. J., Pitkeathly, M., Campbell, I. D., and Dobson, C. M. (1998) The folding kinetics and thermodynamics of the Fyn-SH3 domain, *Biochemistry 37*, 2529−2537.
54. Guijarro, J. I., Morton, C. J., Plaxco, K. W., Campbell, I. D., and Dobson, C. M. (1998) Folding kinetics of the SH3 domain of PI3 kinase by real-time NMR combined with optical spectroscopy, *J. Mol. Biol. 276*, 657−667.
55. Grantcharova, V. P., and Baker, D. (1997) Folding dynamics of the Src SH3 domain, *Biochemistry 36*, 15685−15692.
56. Viguera, A. R., Martinez, J. C., Filimonov, V. V., Mateo, P. L., and Serrano, L. (1994) Thermodynamic and kinetic analysis of the SH3 domain of spectrin shows a two-state folding transition, *Biochemistry 33*, 2142−2150.
57. Bateman, A., Coin, L., Durbin, R., Finn, R. D., Hollich, V., Griffiths-Jones, S., Khanna, A., Marshall, M., Moxon, S., Sonnhammer, E. L., Studholme, D. J., Yeats, C., and Eddy, S. R. (2004) The Pfam protein families database, *Nucleic Acids Res. 32*, D138−D141.
58. Ghose, R., Shekhtman, A., Goger, M. J., Ji, H., and Cowburn, D. (2001) A novel, specific interaction involving the Csk SH3 domain and its natural ligand, *Nat. Struct. Biol. 8*, 998−1004.
59. Lee, C. H., Saksela, K., Mirza, U. A., Chait, B. T., and Kuriyan, J. (1996) Crystal structure of the conserved core of HIV-1 Nef complexed with a Src family SH3 domain, *Cell 85*, 931−942.
60. Clackson, T., and Wells, J. A. (1995) A hot spot of binding energy in a hormone−receptor interface, *Science 267*, 383−386.
61. Manser, E., Loo, T. H., Koh, C. G., Zhao, Z. S., Chen, X. Q., Tan, L., Tan, I., Leung, T., and Lim, L. (1998) PAK kinases are directly coupled to the PIX family of nucleotide exchange factors, *Mol. Cell. Biol. 1*, 183−192.

62. Mongiovi, A. M., Romano, P. R., Panni, S., Mendoza, M., Wong, W. T., Musacchio, A., Cesareni, G., and Di Fiore, P. P. (1999) A novel peptide−SH3 interaction, *EMBO J. 18*, 5300−5309.
63. Liu, Q., Berry, D., Nash, P., Pawson, T., McGlade, C. J., and Li, S. S. (2003) Structural basis for specific binding of the Gads SH3 domain to an RxxK motif-containing SLP-76 peptide: A novel mode of peptide recognition, *Mol. Cell. 11*, 471−481.
64. Kato, M., Miyazawa, K., and Kitamura, N. (2000) A deubiquitinating enzyme UBPY interacts with the Src homology 3 domain of Hrs-binding protein via a novel binding motif PX(V/I)(D/N)-RXXKP, *J. Biol. Chem. 275*, 37481−37487.
65. Petosa, C., Schoehn, G., Askjaer, P., Bauer, U., Moulin, M., Steuerwald, U., Soler-Lopez, M., Baudin, F., Mattaj, I. W., and Muller, C. W. (2004) Architecture of CRM1/exportin1 suggests how cooperativity is achieved during formation of a nuclear export complex, *Mol. Cell 16*, 761−775.
66. Haslbeck, M., Franzmann, T., Weinfurtner, D., and Buchner, J. (2005) Some like it hot: The structure and function of small heat-shock proteins, *Nat. Struct. Mol. Biol. 12*, 842−846.
67. Spiess, C., Meyer, A. S., Reissmann, S., and Frydman, J. (2004) Mechanism of the eukaryotic chaperonin: Protein folding in the chamber of secrets, *Trends Cell Biol. 14*, 598−604.
68. Barila, D., and Superti-Furga, G. (1998) An intramolecular SH3-domain interaction regulates c-Abl activity, *Nat. Genet. 18*, 280−282.
69. Andreotti, A. H., Bunnell, S. C., Feng, S., Berg, L. J., and Schreiber, S. L. (1997) Regulatory intramolecular association in a tyrosine kinase of the Tec family, *Nature 385*, 93−97.
70. Groemping, Y., Lapouge, K., Smerdon, S. J., and Rittinger, K. (2003) Molecular basis of phosphorylation-induced activation of the NADPH oxidase, *Cell 113*, 343−355.
71. Laederach, A., Cradic, K. W., Fulton, D. B., and Andreotti, A. H. (2003) Determinants of intra versus intermolecular self-association within the regulatory domains of Rlk and Itk, *J. Mol. Biol. 329*, 1011−1020.
72. Maignan, S., Guilloteau, J. P., Fromage, N., Arnoux, B., Becquart, J., and Ducruix, A. (1995) Crystal structure of the mammalian Grb2 adaptor, *Science 268*, 291−293.
73. Kishan, K. V., Newcomer, M. E., Rhodes, T. H., and Guilliot, S. D. (2001) Effect of pH and salt bridges on structural assembly: Molecular structures of the monomer and intertwined dimer of the Eps8 SH3 domain, *Protein Sci. 10*, 1046−1055.

BI060590Z